Computational Geosciences (2018) 22:1423–1432
https://doi.org/10.1007/s10596-018-9761-5

ORIGINAL PAPER

A single-relaxation-time lattice Boltzmann model for anisotropic advection-diffusion equation based on the diffusion velocity flux formulation

Janez Perko[1]

Received: 6 November 2017 / Accepted: 11 July 2018 / Published online: 19 July 2018

Abstract

In this paper, we describe a single-relaxation-time (SRT) lattice Boltzmann formulation, which can be effectively applied to anisotropic advection-dispersion equations (AADE). The formulation can be applied to space and time variable anisotropic hydrodynamic dispersion tensor. The approach utilizes diffusion velocity lattice Boltzmann formulation which in the case of AADE can represent anisotropic diagonal and off-diagonal elements of the dispersion matrix by the coupling of advective and diffusive fluxes in equilibrium function. With this approach, AADE can be applied to the SRT lattice Boltzmann formulation using the same equilibrium function and without any changes to collision step nor in the application of boundary conditions. The approach shows good stability even for highly anisotropic dispersion tensor and is tested on selected illustrative examples which demonstrate the accuracy and applicability of the proposed method.

Keywords Lattice Boltzmann method · Anisotropic advection-dispersion equation · Single relaxation time · Diffusion velocity flux

Mathematics Subject Classification (2010) 47.56.+r · 47.11.-j

1 Introduction

In recent years, the lattice Boltzmann method has proven to be very effective approach in the simulation of flow and transport porous media at the pore scale, due to its inherent ability to handle very complex geometries. The purpose of such studies is to gain understanding on process-level [5, 18, 20] or to perform upscaling of physical properties from pore to continuum scale, i.e., effective properties [6, 7, 24]. However, LBM can be also applied to model processes on continuum scale [16, 28] using bulk physical properties such as porosity, effective diffusion, permeability, or hydrodynamic dispersion. Hydrodynamic dispersion plays an important role in macroscopic advective-dispersion transport phenomena in porous media and is usually conceptualized by two separate mechanisms, namely molecular diffusion and mechanical dispersion. The importance of dispersion in solute transport is recognized and studied thoroughly in many fields [5, 13, 19]. Molecular diffusion occurs as a result of thermal motion of the molecules. Mechanical dispersion, on the other hand, is a result of different water flow paths resulting from different pore sizes, orientation, and trace lengths. Physically, the mechanical dispersion can be the product of advective velocity and the dispersion [2], but it can also depend on concentration [23] or saturation degree [22].

In its original form, the single-relaxation-time (SRT) lattice Boltzmann models for advective-diffusive (dispersion) equation are limited to the description of isotropic diffusion problems. This is based on the fact that in SRT (also termed BGK formulation), only a single relaxation process is used to characterize the collision effects. In other words, all modes relax to their equilibria with the same rate. In the case of classical SRT formulation, the dissipation parameter can only be a scalar value, while anisotropic

✉ Janez Perko
jperko@sckcen.be

[1] Institute for Environment Health and Safety, Engineered and Geosystems Analysis, Belgian Nuclear Research Centre SCK · CEN, Mol, Belgium

advective-dispersion equations (AADE) introduces a hydrodynamic dispersion tensor, which requires different relaxation modes during the collision process [17, 32]. Zhang et al. [34] introduced the approach using direction-dependent relaxation parameters which enabled the implementation of anisotropic diffusion within the SRT lattice Boltzmann. The model of Zhang et al. [34] is implemented in SRT and has four relaxation parameters in nine directions. Conservation of mass is ensured by taking a weighted summation of the particle distribution function. This model was used in the example of Karst flows and transport processes [1]. However, in [9], it is argued that the SRT-type construction cannot have a mass conserving equilibrium function when the relaxation parameters differ temporarily. Ginzburg [9] alleviates the problem of mass conservation of [34] by introducing link-wise collision operator. This configuration is called the two-relaxation-time (TRT) operator which retains the simplicity of SRT, but improves its stability and accuracy. Rasin et al. [27] and Yoshida et al. [33] proposed MRT method to incorporate full anisotropy associated with reduced models with five discrete velocities in two dimensions (D2Q5) and seven discrete velocities in three dimensions (D3Q7). All these approaches are combined and investigated for the numerical diffusion and the associated stability towards the anisotropy in work [11]. The multi-relaxation-time (MRT) formulation approach to solve nonlinear AADE is recently presented by [15] or [4]. MRT models involve a number of tunable parameters which can be tuned to improve stability and accuracy, but for a general system, this optimum is not straightforward to determine. The use of non-coordinate discrete velocity stencils for the non-diagonal diffusion terms in the existing SRT and TRT models are alleviated in the present model via the coupling of the advective and diffusive fluxes in the equilibrium function. As demonstrated in this work, the approach offers an easy to implement and accurate way to solve anisotropic physical problems with SRT formulation. The same formulation can be introduced within TRT approach, which would additionally improve the stability and accuracy. The advantage of the new approach are:

- The equilibrium function formulation remains the same as for isotropic problems (i.e., Eq. 5).
- Diffusion velocity formulation is stable for large variations of dissipation parameters and anisotropy ratios.
- Minimal velocity set lattices, D2Q5 or D3Q7, can be used to model fully anisotropic ADE.
- The model is straightforward to implement.

In this work, no additional analysis has been performed in terms of numerical dispersion. Since the formulation of the equilibrium function remains identical to the standard SRT formulation as given in Eq. 5 (with additional velocity resulting from diffusion velocity approach), it is expected that the numerical dispersion due to truncation errors would be similar to the one of SRT. However, in order to compare this method with the known results on the other formulations, similar analysis should be done in future. Boundary conditions can also be applied in the same way as for the classical SRT advection-dispersion equation.

2 Physical and numerical framework

The central physical framework elaborated in this paper is a solute transport in porous media, which is described by advection-dispersion transport equation in Eq. 1.

$$\frac{\partial \theta C}{\partial t} = -\nabla \cdot \mathbf{J} + R \tag{1}$$

$$\mathbf{J} = -\theta\, \mathbf{D}\, \nabla C + \mathbf{u}\, C \tag{2}$$

where C is the concentration $[\mathrm{M\,L^{-3}}]$, $\mathbf{J}$ is the flux $[\mathrm{M\,L^{-2}\,T^{-1}}]$, $\mathbf{D}$ is the hydrodynamic dispersion $[\mathrm{L^2\,T^{-1}}]$, $\mathbf{u}$ is the volume averaged velocity of the fluid $[\mathrm{L\,T^{-1}}]$, and R represents the volumetric source term $[\mathrm{M\,L^{-3}\,T^{-1}}]$. θ is the porosity [-] which is a property of porous media. For the purpose of this article, we simplify the derivation, without loss of generality, to $\theta = 1$. Interested reader can see possible implementations in the existing literature [14, 25, 31].

The focus of this work is in the solution of the macroscopic advection-dispersion transport equation, solved by the lattice Boltzmann method in its simplest form, where the collision term Ω^{SRT} of discrete Boltzmann equation is described by a single relaxation time [3] as:

$$f_i(\mathbf{r} + \mathbf{e_i}\,\Delta t, t + \Delta t) = f_i(\mathbf{r}, t) + \Omega^{SRT}(\mathbf{r}, t) \tag{3}$$

$$\Omega^{SRT}(\mathbf{r}, t) = \frac{\Delta t}{\tau}\left(f_i^{eq}(\mathbf{r}, t) - f_i(\mathbf{r}, t)\right). \tag{4}$$

where $\mathbf{r}$ is the position vector, f_i represents the particle distribution functions along the ith lattice direction in velocity space, $\mathbf{e}$ is the velocity vector in the ith direction, which depends on the type of lattice, Δt is the lattice time step (further derivation and analysis in this work assume $\Delta t = 1$), τ is relaxation time, and f_i^{eq} is the particle equilibrium distribution functions given by:

$$f_i^{eq}(\mathbf{r}, t) = w_i\, C\left(1 + \frac{\mathbf{e_i} \cdot \mathbf{u}}{e_s^2}\right) \tag{5}$$

where w_i are the weights for the particle distribution function along the ith direction, e_s is "pseudo-sound-speed" $[\mathrm{L\,T^{-1}}]$ [21], and $\mathbf{u}$ is the velocity vector in lattice units. The lattice velocity e_s^2 is $e^2/3$ for D2Q5 lattice in our analysis. It is acknowledged that also w_i and e_s^2 are tunable and have an effect to the stability, e.g., [10, 12], but we keep these values constant in this work.

Using the particle equilibrium distribution function given by Eq. 5 on appropriate lattices (D2Q5 in this work), it is possible to recover (1) using the multiscale Chapman-Enskog expansion [8] from which the relation between lattice Boltzmann diffusion coefficient (D) (i.e., diffusion coefficient in lattice units) and relaxation time is defined

$$D = e_s^2 \left(\tau - \frac{1}{2}\right). \tag{6}$$

3 Hydrodynamic dispersion within the diffusion velocity formulation

In [26], a novel idea on the treatment of large contrasts in dissipation parameters has been introduced. This idea is based on the *diffusion velocity* (the name is taken after [30]) where the physical dissipation parameter (e.g., hydrodynamic dispersion) can be divided into a reference value D_{ref}, which is constant over entire domain and a tensor of fluctuating values $\tilde{\mathbf{D}}$ which represents a deviation from the reference. This can be written as

$$\mathbf{D} = D_{\text{ref}}\,\mathbf{I} + \tilde{\mathbf{D}} \tag{7}$$

The reference part is used to define the physical time scale as in Eq. 6 but now with D_{ref} instead of D. The fluctuating part, on the other hand, is transferred to a new velocity (hence termed *diffusion velocity*), which contributes to a new advection term. The whole hydrodynamic dispersion tensor comprises pore diffusion diagonal matrix and a dispersion tensor $\mathbf{D}^*$.

$$\mathbf{D} = \mathbf{I}\cdot\mathbf{D}_p + \mathbf{D}^* \tag{8}$$

Combining (7) and (8), we derive the tensor of fluctuating values $\tilde{\mathbf{D}}$

$$\tilde{\mathbf{D}} = \mathbf{I}\cdot\mathbf{D}_p - D_{ref}\,\mathbf{I} + \mathbf{D}^* \tag{9}$$

where $\mathbf{D}_p$ is the pore water diffusion coefficient with $\{D_{p,x}, D_{p,y}, D_{p,z}\}$ components in three dimensions. The fluctuation tensor in 3D in Eq. 9 reads:

$$\tilde{\mathbf{D}} = \begin{vmatrix} \tilde{D}_{xx} & \tilde{D}_{xy} & \tilde{D}_{xz} \\ \tilde{D}_{yx} & \tilde{D}_{yy} & \tilde{D}_{yz} \\ \tilde{D}_{zx} & \tilde{D}_{zy} & \tilde{D}_{zz} \end{vmatrix} \tag{10}$$

and expansion by Eq. 9 gives

$$\tilde{\mathbf{D}} = \begin{vmatrix} D_{p,x} - D_{ref} + D^*_{xx} & D^*_{xy} & D^*_{xz} \\ D^*_{yx} & D_{p,y} - D_{ref} + D^*_{yy} & D^*_{yz} \\ D^*_{zx} & D^*_{zy} & D_{p,z} - D_{ref} + D^*_{zz} \end{vmatrix}. \tag{11}$$

The diffusion velocity is derived from the assumption that the total flux in the system $\mathbf{J}$ remains constant and mass fluxes belonging to the fluctuating part are expressed by advective flux (see [26]) as described by Eq. 12.

$$C\,\mathbf{u}_d = -\tilde{\mathbf{D}}\nabla C, \tag{12}$$

where $\mathbf{u}_d$ is the diffusion velocity. Using Eqs. 12 and 7, we can express the total flux in Eq. 2 by diffusive fluxes associated with the reference diffusion, with the fluctuating dispersion tensor expressed as the diffusion velocity flux resulting from diffusion velocity $\mathbf{u}_d$ and by the flux resulting from fluid flow defined by field velocity $\mathbf{u}_a$.

$$\mathbf{J} = -\mathbf{I}\,D_{\text{ref}}\,\nabla C - \tilde{\mathbf{D}}\,\nabla C + C\,\mathbf{u}_a = -\mathbf{I}\,D_{\text{ref}}\,\nabla C + C\,(\mathbf{u}_d + \mathbf{u}_a) \tag{13}$$

Substitution of Eqs. 10 to Eq. 12 yields for Cartesian $\beta \in \{x, y, z\}$ components

$$\begin{aligned} C\,u_{d,x} &= -\left(\tilde{D}_{xx}\frac{\partial C}{\partial x} + \tilde{D}_{xy}\frac{\partial C}{\partial y} + \tilde{D}_{xz}\frac{\partial C}{\partial z}\right) \\ C\,u_{d,y} &= -\left(\tilde{D}_{xy}\frac{\partial C}{\partial x} + \tilde{D}_{yy}\frac{\partial C}{\partial y} + \tilde{D}_{yz}\frac{\partial C}{\partial z}\right) \\ C\,u_{d,z} &= -\left(\tilde{D}_{xz}\frac{\partial C}{\partial x} + \tilde{D}_{yz}\frac{\partial C}{\partial y} + \tilde{D}_{zz}\frac{\partial C}{\partial z}\right) \end{aligned} \tag{14}$$

Within the LB framework, the diffusion velocity is derived from the first-order expansion terms of the Chapman-Enskog multiscale expansion, which represent mass conservation. The concentration gradients are locally calculated neglecting second and higher order terms as

$$\frac{\partial C}{\partial x_\beta} \approx -\frac{1}{\tau\, e_s^2}\left(\sum_i f_i\, e_{i\,\beta} - C\,(u_{a,\beta} + u_{d,\beta})\right). \tag{15}$$

with diffusion velocity $u_{d,\beta}$ and in case of advection-driven transport, field velocity $u_{a,\beta}$. Hence, $u_\beta = u_{d,\beta} + u_{a,\beta}$. Spatial derivatives in Eq. 14 can be expanded by the calculation of gradients defined in Eq. 15 for the diffusion velocity fluxes:

$$\begin{aligned} C\,u_{d,x} = -\frac{1}{\tau\, e_s^2}\Bigg(& \tilde{D}^*_{xx}\left(\sum_i f_i\, e_{i\,x} - C\,(u_{a,x} - u_{d,x})\right) + \\ & \tilde{D}^*_{xy}\left(\sum_i f_i\, e_{i\,y} - C\,(u_{a,y} - u_{d,y})\right) + \\ & \tilde{D}^*_{xz}\left(\sum_i f_i\, e_{i\,z} - C\,(u_{a,z} - u_{d,z})\right)\Bigg) \\ C\,u_{d,y} = -\frac{1}{\tau\, e_s^2}\Bigg(& \tilde{D}^*_{yx}\left(\sum_i f_i\, e_{i\,x} - C\,(u_{a,x} - u_{d,x})\right) + \\ & \tilde{D}^*_{yy}\left(\sum_i f_i\, e_{i\,y} - C\,(u_{a,y} - u_{d,y})\right) + \\ & \tilde{D}^*_{yz}\left(\sum_i f_i\, e_{i\,z} - C\,(u_{a,z} - u_{d,z})\right)\Bigg) \\ C\,u_{d,z} = -\frac{1}{\tau\, e_s^2}\Bigg(& \tilde{D}^*_{zx}\left(\sum_i f_i\, e_{i\,x} - C\,(u_{a,x} - u_{d,x})\right) + \\ & \tilde{D}^*_{zy}\left(\sum_i f_i\, e_{i\,y} - C\,(u_{a,y} - u_{d,y})\right) + \\ & \tilde{D}^*_{zz}\left(\sum_i f_i\, e_{i\,z} - C\,(u_{a,z} - u_{d,z})\right)\Bigg) \end{aligned} \tag{16}$$

Hence, the diffusion velocities for all components can be determined by solving the system of equations in Eq. 16 for the diffusion velocity fluxes $C\,u_{d,x}$, $C\,u_{d,y}$, and $C\,u_{d,z}$.

$$C\,u_{x,d} = \mathcal{F}_x - \frac{\det\begin{bmatrix}\mathcal{F}_x & 0 & 0\\ 0 & (1+\mathcal{D}_{yy}) & \mathcal{D}_{yz}\\ 0 & \mathcal{D}_{zy} & (1+\mathcal{D}_{zz})\end{bmatrix}}{\Psi} + \frac{\det\begin{bmatrix}\mathcal{D}_{xy} & 0 & \mathcal{D}_{xz}\\ 0 & \mathcal{F}_y & 0\\ \mathcal{D}_{zy} & 0 & (1+\mathcal{D}_{zz})\end{bmatrix}}{\Psi} + \frac{\det\begin{bmatrix}\mathcal{D}_{xz} & \mathcal{D}_{xy} & 0\\ \mathcal{D}_{yz} & (1+\mathcal{D}_{yy}) & 0\\ 0 & 0 & \mathcal{F}_z\end{bmatrix}}{\Psi} \tag{17}$$

$$C\,u_{y,d} = \mathcal{F}_y + \frac{\det\begin{bmatrix}\mathcal{F}_x & 0 & 0\\ 0 & \mathcal{D}_{yx} & \mathcal{D}_{yz}\\ 0 & \mathcal{D}_{zx} & (1+\mathcal{D}_{zz})\end{bmatrix}}{\Psi} - \frac{\det\begin{bmatrix}(1+\mathcal{D}_{xx}) & 0 & \mathcal{D}_{xz}\\ 0 & \mathcal{F}_y & 0\\ \mathcal{D}_{zx} & 0 & (1+\mathcal{D}_{zz})\end{bmatrix}}{\Psi} + \frac{\det\begin{bmatrix}(1+\mathcal{D}_{xx}) & \mathcal{D}_{xz} & 0\\ \mathcal{D}_{yx} & \mathcal{D}_{yz} & 0\\ 0 & 0 & \mathcal{F}_z\end{bmatrix}}{\Psi} \tag{18}$$

$$C\,u_{z,d} = \mathcal{F}_z + \frac{\det\begin{bmatrix}\mathcal{F}_x & 0 & 0\\ 0 & (1+\mathcal{D}_{yy}) & \mathcal{D}_{zy}\\ 0 & \mathcal{D}_{yx} & \mathcal{D}_{zx}\end{bmatrix}}{\Psi} + \frac{\det\begin{bmatrix}(1+\mathcal{D}_{xx}) & 0 & \mathcal{D}_{xy}\\ 0 & \mathcal{F}_y & 0\\ \mathcal{D}_{zx} & 0 & \mathcal{D}_{zy}\end{bmatrix}}{\Psi} - \frac{\det\begin{bmatrix}(1+\mathcal{D}_{xx}) & \mathcal{D}_{xy} & 0\\ \mathcal{D}_{yx} & (1+\mathcal{D}_{yy}) & 0\\ 0 & 0 & \mathcal{F}_z\end{bmatrix}}{\Psi} \tag{19}$$

where we introduced the following variables for the purpose of shorter notation:

$$\mathcal{D} = \tilde{\mathbf{D}}^* \frac{1}{\tau\, e_s^2}$$

$$\mathcal{F}_\beta = \sum_i f_i\, e_{i\,\beta} - C\,u_{a,\beta}$$

and

$$\Psi = \det\begin{bmatrix}(1+\mathcal{D}_{xx}) & \mathcal{D}_{xy} & \mathcal{D}_{xz}\\ \mathcal{D}_{yx} & (1+\mathcal{D}_{yy}) & \mathcal{D}_{yz}\\ \mathcal{D}_{zx} & \mathcal{D}_{zy} & (1+\mathcal{D}_{zz})\end{bmatrix}$$

If $\mathcal{D}$ values remain the same (e.g., in a constant flow field), these values need to be calculated only one time. On the other hand, $\mathcal{F}$ values depend on the concentration gradient and need to be calculated at each time step. Expanded 2D expression (with x and y components) significantly simplifies to:

$$C\,u_{x,d} = \frac{\mathcal{D}_{xx}\,\mathcal{F}_x + \mathcal{D}_{xy}\,\mathcal{F}_y - \frac{\mathcal{D}_{xy}}{(1+\mathcal{D}_{yy})}\,(\mathcal{D}_{yy}\,\mathcal{F}_y + \mathcal{D}_{yx}\,\mathcal{F}_x)}{\left(1+\mathcal{D}_{xx} - \frac{\mathcal{D}_{xy}\,\mathcal{D}_{yx}}{1+\mathcal{D}_{yy}}\right)}$$

$$C\,u_{y,d} = \frac{\mathcal{D}_{yy}\,\mathcal{F}_y + \mathcal{D}_{yx}\,\mathcal{F}_x - \frac{\mathcal{D}_{yx}}{(1+\mathcal{D}_{xx})}\,(\mathcal{D}_{xx}\,\mathcal{F}_x + \mathcal{D}_{xy}\,\mathcal{F}_y)}{\left(1+\mathcal{D}_{yy} - \frac{\mathcal{D}_{xy}\,\mathcal{D}_{yx}}{1+\mathcal{D}_{xx}}\right)} \tag{20}$$

The velocity vector calculated from the directional velocities in Eq. 17 or Eq. 20 for the 3D and 2D problem, respectively is used in the calculation of the equilibrium function (5) as an additional advective term:

$$f_i^{eq}(\mathbf{r},t) = w_i\, C\left(1 + \frac{\mathbf{e_i}\cdot(\mathbf{u}_a + \mathbf{u}_d)}{e_s^2}\right) \tag{21}$$

where $C\,\mathbf{u}_d$ is calculated in Eqs. 17–20.

It should be noted that the presented formulation reduces to the original SRT lattice Boltzmann method when $D_{\text{ref}} = D_p$ for an isotropic system and all properties of the method in terms of accuracy and stability apply to the original SRT formulation. D_{ref} is a free parameter, which can be tuned to define the time step in the same way as diffusion in the original SRT model.

3.1 Numerical results and discussion

Two numerical examples are shown to demonstrate the ability and accuracy of the presented formulation. The first example is a dispersion of a Gaussian hill, which is often used to validate the numerical method as already demonstrated in [4, 11, 15]. The second example demonstrates the applicability of the formulation on spatially variable flow field and dispersion tensor with higher Pe number.

3.1.1 Anisotropic dispersion with spatially constant velocity

The Gaussian hill problem considers a source within a domain which is transported by spatially constant velocity

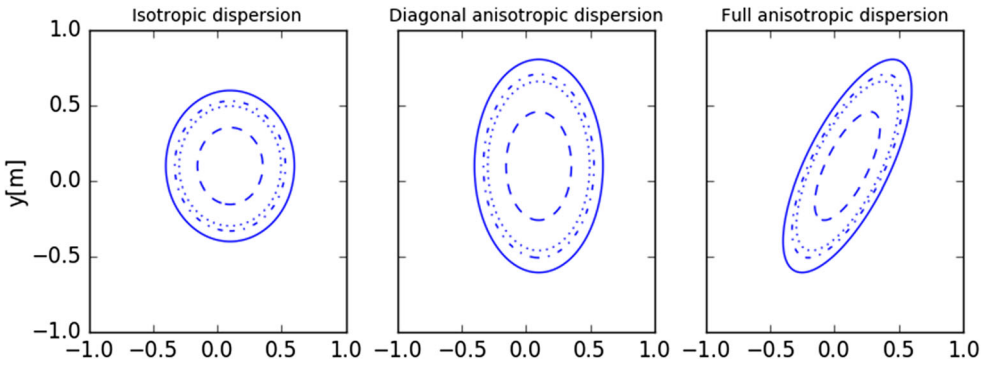

Fig. 1 Contours of the Gaussian hill problem at time 10 s. Values of contours of a scalar variable are 10^{-5} (full), $5{\cdot}10^{-5}$ (dash-dot), 10^{-4} (dotted), 10^{-3} (dashed)

and diffusion tensor within Eq. 1. Initially, the concentration is defined by

$$C(x, y, t = 0) = \exp^{-\frac{(x^2+y^2)}{2C_0^2}} \tag{22}$$

For this example, under given boundary and initial conditions, an analytical solution in Eq. 23 exists for this problem.

$$C(x, y, t) = \frac{C_0}{|\det(\sigma)|^{1/2}} \left(-\frac{\sigma^{-1} : ((\mathbf{x} - \mathbf{u}_a\, t)(\mathbf{x} - \mathbf{u}_a\, t)^{\mathsf{T}})}{2} \right) \tag{23}$$

where $\mathbf{x} = (x, y)^{\mathsf{T}}$, $\mathbf{u}_a = (u_{x,a}, u_{y,a})^{\mathsf{T}}$ and $\sigma = C_0^2\,\mathbf{I} + 2\,\mathbf{D}\,t$, σ^{-1} is inverse matrix of σ, and $\det\sigma$ is the determinant of σ. The problem domain is bounded within $[-1, 1] \times [-1, 1]$ [m] and results are compared at time $t = 10$ s at which the boundary conditions can be defined as zero flux or periodic boundary conditions. $C_0 = 0.01$ and velocity vector components are $\mathbf{u}_a = (0.01, 0.01)$ m/s. The ability of the present formulation to solve AADE is shown in Fig. 1 for the three types of dispersion tensor as in [4] as given in Eq. 24.

$$\mathbf{D} = \left(\begin{bmatrix} 1 & 0 \\ 0 & 1 \end{bmatrix}, \begin{bmatrix} 1 & 0 \\ 0 & 2 \end{bmatrix}, \begin{bmatrix} 1 & 1 \\ 1 & 2 \end{bmatrix} \right) \times 10^{-3} \mathrm{m}^2/s \tag{24}$$

For the analysis of accuracy, the global relative error (GRE) defined by Eq. 25 and maximal error defined by Eq. 26 are used:

$$\mathrm{GRE} = \frac{\sum_i \left| C(\mathbf{r}, t)_{\mathrm{analytic}} - C(\mathbf{r}, t)_{\mathrm{numeric}} \right|}{\sum_i \left| C(\mathbf{r}, t)_{\mathrm{analytic}} \right|}, \tag{25}$$

$$\mathrm{Err}_{\max} = \max \left| C(\mathbf{r}, t)_{\mathrm{analytic}} - C(\mathbf{r}, t)_{\mathrm{numeric}} \right|. \tag{26}$$

The values in Table 1 are given for different nodal distances (space discretization) $\Delta x = 0.02, 0.01, 0.005, 0.0033, 0.0025$ m corresponding to the number of nodes $N = 100 \times 100, 200 \times 200, 400 \times 400, 600 \times 600, 800 \times 800$, respectively in a square domain $\{-1, 1\} \times \{-1, 1\}$ in order to determine the rate of convergence.

From Fig. 2, it can be seen that the mesh convergence is of second order. The error is slightly lower for the isotropic case than for diagonally and fully anisotropic case, which is similar to the MRT results shown in [4] but with lower differences between different levels of dispersion tensor anisotropies.

Diffusion velocity formulation has two free parameters, the reference diffusion coefficient D_{ref} and the relaxation time τ. The time step can be controlled by changing D_{ref} and keeping the relaxation time τ constant or changing the relaxation time τ while keeping D_{ref} constant or adapting both. Figure 3 presents the first two cases with keeping either D_{ref} or τ constant. The stability and accuracy are studied for different Péclet numbers for the fully anisotropic

Table 1 Global relative error and maximum error for three analyzed cases

Δx	GRE	$\mathrm{Err}_{\max}$
	Isotropic dispersion	
0.02	$3.46{\cdot}10^{-2}$	$1.63{\cdot}10^{-4}$
0.01	$8.49{\cdot}10^{-4}$	$3.14{\cdot}10^{-6}$
0.005	$2.10{\cdot}10^{-4}$	$7.82{\cdot}10^{-7}$
0.0033	$9.30{\cdot}10^{-5}$	$3.46{\cdot}10^{-7}$
0.0025	$5.22{\cdot}10^{-5}$	$1.94{\cdot}10^{-7}$
	Diagonal anisotropic dispersion	
0.02	$3.46{\cdot}10^{-2}$	$1.14{\cdot}10^{-4}$
0.01	$1.20{\cdot}10^{-3}$	$3.73{\cdot}10^{-6}$
0.005	$2.98{\cdot}10^{-4}$	$9.23{\cdot}10^{-7}$
0.0033	$1.34{\cdot}10^{-4}$	$4.09{\cdot}10^{-7}$
0.0025	$8.14{\cdot}10^{-6}$	$5.35{\cdot}10^{-6}$
	Full anisotropic dispersion	
0.02	$3.59{\cdot}10^{-2}$	$1.66{\cdot}10^{-4}$
0.01	$2.04{\cdot}10^{-3}$	$8.31{\cdot}10^{-6}$
0.005	$5.07{\cdot}10^{-4}$	$2.06{\cdot}10^{-6}$
0.0033	$2.26{\cdot}10^{-4}$	$9.13{\cdot}10^{-7}$
0.0025	$1.28{\cdot}10^{-4}$	$5.13{\cdot}10^{-7}$

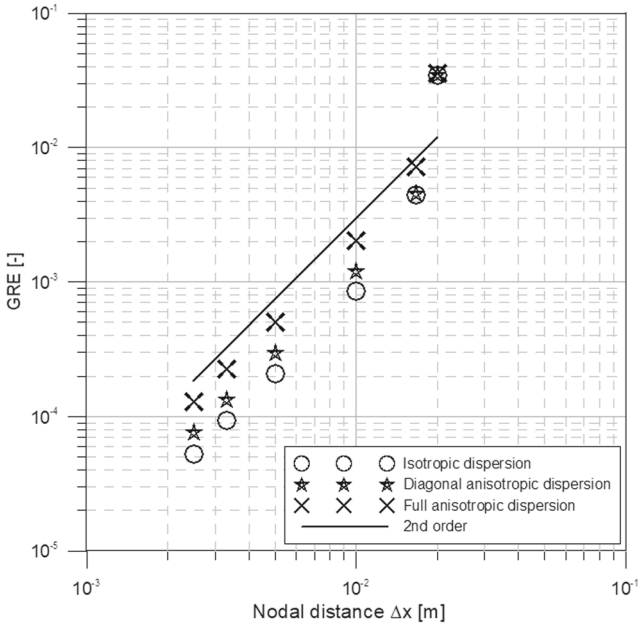

Fig. 2 Global relative error at different lattice spacing. 1st and 2nd lines represent the order of mesh convergence

case of Eq. 24 on 200 × 200 mesh. The local Péclet number for fully anisotropic dispersion case in 2D is calculated as

$$Pe = \frac{\|\mathbf{u}\|\,\Delta x\,(u_x^2 + u_y^2)^{3/2}}{D_{xx}\,u_x^2 + D_{xy}\,u_x\,u_y + D_{yx}\,u_x\,u_y + D_{yy}\,u_y^2}$$

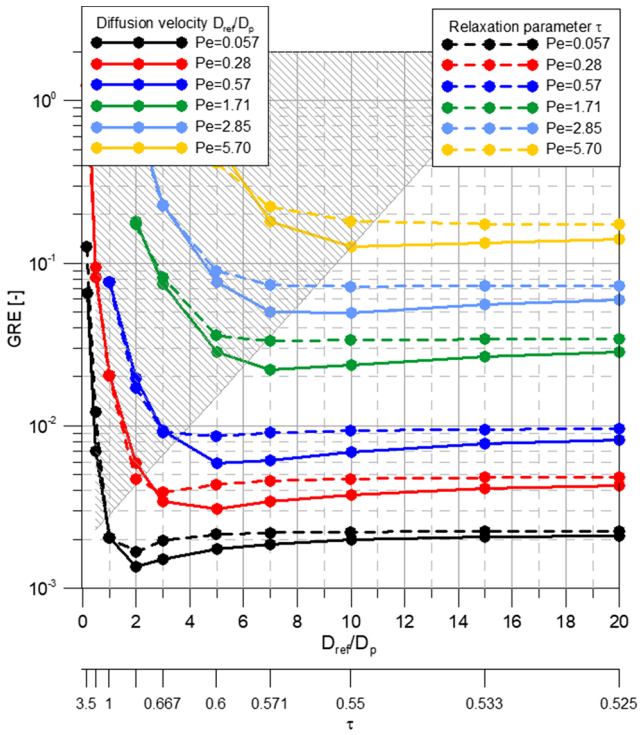

Fig. 3 Global relative error and stability at various Péclet numbers for different D_{ref}/D_p ratios and variations of the relaxation time τ

The above definition of Péclet number is taken from COMSOL Multiphysics software because the last analysis with anisotropic dispersion with spatially varying velocities is compared with this modeling tool.

The behavior of both approaches (by changing either D_{ref} or τ) in terms of errors is shown in Fig. 3 for different local (mesh) Péclet numbers: $Pe = 0.057$ based on $u = 0.01$ m/s, $Pe = 0.28$ based on $u = 0.05$ m/s, $Pe = 0.57$ based on $u = 0.1$ m/s, $Pe = 1.71$ based on $u = 0.3$ m/s, $Pe = 2.85$ based on $u = 0.5$ m/s, and $Pe = 5.7$ based on $u = 1.0$ m/s. The dispersion matrix is the same as given in Eq. 24, and diffusion is $D_p = 10^{-3}$ m^2/s. In order to ensure that the Gaussian hill remains within the domain at different Pe numbers, the final time is adapted as follows: $t = 10$ s for $Pe = 0.057$, $t = 6$ s for $Pe = 0.28$, $t = 4$ s for $Pe = 0.57$, $t = 2$ s for $Pe = 1.71$, $t = 1$ s for $Pe = 2.85$, and $t = 0.5$ s for $Pe = 5.7$.

The results for diffusion velocity formulation in Fig. 3 are denoted by full lines for D_{ref}/D_p ratios of 1/6, 1/2, 1, 2, 3, 5, 7, 10, 15, and 20 and $\tau = 1$. For comparison, we computed results by changing the relaxation time τ in such a way that the number of time steps for each case is the same as for the diffusion velocity cases resulting in τ 3.5, 1.5, 1, 0.75, 0.667, 0.6, 0.5714, 0.555, 0.5333, and 0.525 while keeping $D_{\text{ref}} = D_p$. These results are denoted by dashed lines in Fig. 3. The comparison shows that the accuracy of the model changes decreases with larger Pe. The exponential trend is similar for both, diffusion velocity and relaxation time, approaches. However, in a stable region, the accuracy of diffusion velocity formulation is up to two times better than when using the relaxation time formulation, especially for the cases with higher Pe. Hence, it is preferred to vary D_{ref} and fix the relaxation time τ. The stability region is similar for both approaches

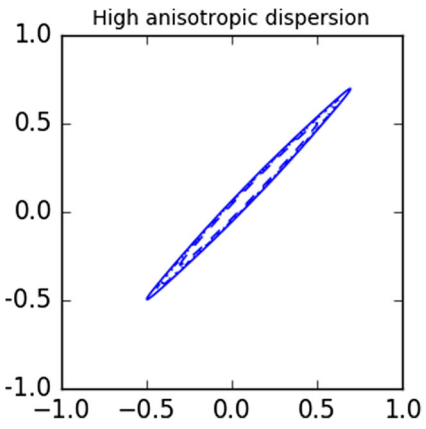

Fig. 4 Contour plots for advection-dispersion equation at time 10 s of the 2D Gaussian hill at the anisotropic limit: $D_{xx} = D_{yy} = D_{xy} = D_{yx} = 10^{-3}$ m^2/s. Values of contours of a scalar variable are 10^{-5} (full), $5{\cdot}10^{-5}$ (dash-dot), 10^{-4} (dotted), 10^{-3} (dashed)

and approximately denoted by gray shaded region when the calculations were not stable.

As described in [11], the theoretical anisotropic limit is when the off-diagonal dispersion tensor elements are equal to the diagonal ones. To test the ability of the proposed model to simulate highly anisotropic tensors, which results in sharp concentration gradients, is demonstrated in Fig. 4. The simulation is made for the dispersion matrix $D_{xx} = D_{yy} = D_{xy} = D_{yx} = 10^{-3}$ m^2/s using 400×400 nodes in the domain size $\mathbf{x} \in \{-1, 1\}$ m. The tuning parameters are set to $D_{\text{ref}} = D_p = 10^{-3}$ m^2/s and $\tau = 1$.

The results show a very good agreement between the theoretical and numerical results.

3.1.2 Anisotropic dispersion with spatially varying velocity

The full potential of the proposed model is illustrated with a numerical example with a spatially variable flow pattern. The test problem devised by Smith and Hutton [29] is defined with convection and diffusion of a scalar field in a prescribed velocity field, $u(x, y, z)$ with a constant D_p. The Smith and Hutton problem was originally proposed for the estimation of numerical diffusion, but in this work, it is applied for the analysis of hydrodynamic dispersion. The problem is defined in quasi 3D with invariant z-direction. Hence, the problem can be defined in x–y plane only. The velocity field is derived from a stream function $\psi = (1 - x^2)(1 - y^2)$. From this stream function, the velocities component in the x-, y-, and z-direction are

$$u_x = -\frac{\psi}{y} = 2\,y\,(1 - x^2);\; x \in [-1, 1],\; y \in [0, 1] \qquad (27)$$

$$u_y = \frac{\psi}{x} = -2\,x\,(1 - y^2)$$

$$u_z = 0$$

The flow domain considered is a rectangle with dimensions $-1 \leq x[\text{m}] \leq 1$ and $0 \leq y[\text{m}] \leq 1$ as shown in Fig. 5. Concentration is defined along the left bottom boundary ($-1 \leq x[\text{m}] \leq 0$, $y = 0$ m). The other part of the bottom boundary ($0 \leq x[\text{m}] \leq 1$, $y = 0$ m) is defined by open boundary. As the original goal was to quantify numerical diffusion of a specific numerical scheme, Smith and Hutton defined a sharp pulse-like shape of the scalar variable from 0 to 1 at the middle of the boundary ($-1 \leq x[\text{m}] \leq 0$, $y = 0$ m). Because of the symmetrical flow field, solute is transported across the domain from the boundary $-1 \leq x[\text{m}] \leq 0$, $y = 0$ m to the other side $0 < x[\text{m}] \leq 1$, $y = 0$ m where the concentration profile is recorded. In this numerical example, the focus is on the verification of numerical scheme with a problem where the dissipation plays an essential role. Further, no specific model accuracy analysis is made because the results are compared between the two numerical models. The inlet concentration profile is symmetrical with respect to the boundary ($-1 \leq x[\text{m}] \leq 0$, $y = 0$ m) in order to see the effect of a varying fluid flow magnitude and direction which results in an asymmetrical profile at the outflow. The boundary concentration is defined as

$$C(x, t) = \frac{\tanh(\Upsilon\,(0.6 + x)) - \tanh(\Upsilon\,(0.4 + x))}{2};\; x \in [-1, 0]$$

where the parameter Υ defines the sharpness of the concentration profile transition. For our example, we used value of $\Upsilon = 100$, which results in a sharp profile. The right portion of the bottom boundary ($x \in [0, 1]$) is an open boundary. All other boundaries are Neumann boundaries with zero flux.

Multiple numerical examples are shown for the demonstration, each one with a specific set of transversal dispersivity coefficient, α_T and longitudinal dispersivity coefficient, α_L. The dispersion tensor $\mathbf{D}^*$ is in an explicit form for the x-, y-, and z-direction in the Cartesian three-dimensional coordinate system.

$$D^*_{xx} = \frac{1}{\bar{u}}\left[\alpha_T\,(u_y^2 + u_z^2) + \alpha_L\,u_x^2\right] \qquad (28)$$

$$D^*_{yy} = \frac{1}{\bar{u}}\left[\alpha_T\,(u_x^2 + u_z^2) + \alpha_L\,u_y^2\right]$$

$$D^*_{zz} = \frac{1}{\bar{u}}\left[\alpha_T\,(u_x^2 + u_y^2) + \alpha_L\,u_z^2\right]$$

$$D^*_{xy} = D^*_{yx} = \frac{u_x\,u_y}{\bar{u}}\left[\alpha_L - \alpha_T\right]$$

$$D^*_{xz} = D^*_{zx} = \frac{u_x\,u_z}{\bar{u}}\left[\alpha_L - \alpha_T\right]$$

$$D^*_{yz} = D^*_{zy} = \frac{u_y\,u_z}{\bar{u}}\left[\alpha_L - \alpha_T\right]$$

$\bar{u}$ is the velocity magnitude, defined as $\sqrt{u_x^2 + u_y^2 + u_z^2}$.

Diffusion coefficient D_p is set to $5 \cdot 10^{-4}$ m^2/day. The domain is discretized in 200×100 nodes. Relaxation time τ is set to 1, while D_{ref} is $5 \cdot 10^{-2}$ m^2/day. Boundary

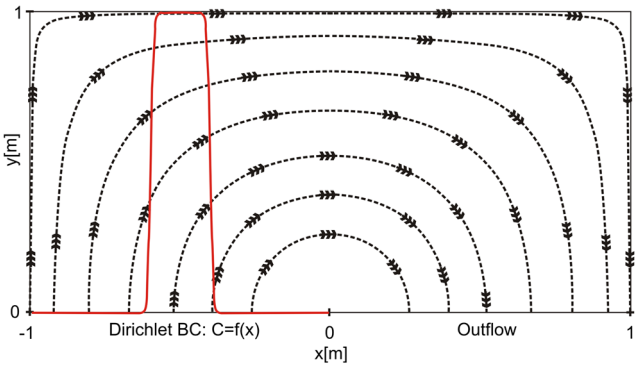

Fig. 5 Calculation domain with streamlines (black dotted line) indicating the direction of flow field and boundary concentration profile (red full line)

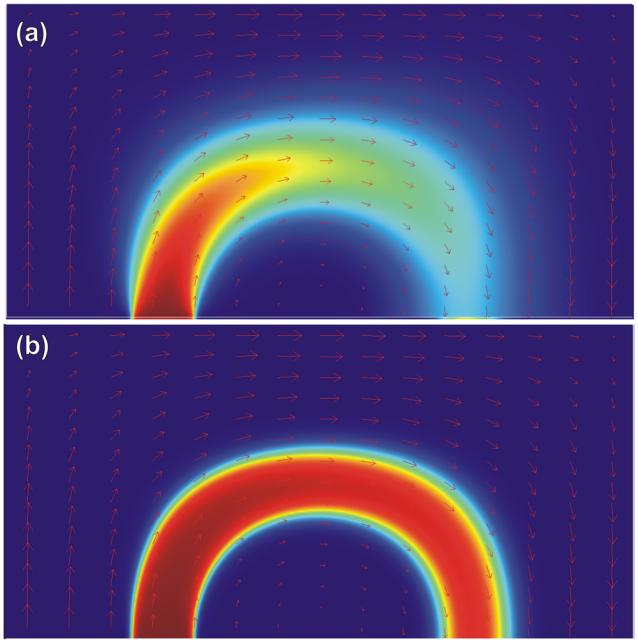

Fig. 6 Concentration field at time 1.7 days for the case with **a** $\alpha_L = 0.1$ m and $\alpha_T = 0.01$ m and **b** $\alpha_L = 1$ m and $\alpha_T = 0.001$ m. Color scale is denoted with blue and red colors for 0 and 1 concentrations, respectively. Red arrows denote the direction and magnitude of flow field

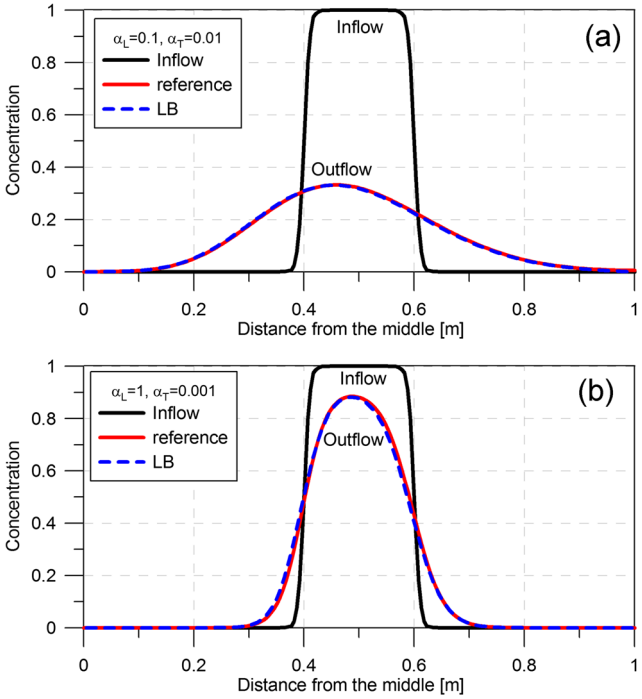

Fig. 7 Concentration at the inlet and outlet boundary at 1.7 days for the case with **a** $\alpha_L = 0.1$ m and $\alpha_T = 0.01$ m and **b** $\alpha_L = 1$ m and $\alpha_T = 0.001$ m

profiles at $0 \leq x[\text{m}] \leq 1$ and $y = 0$ m are shown at 1.7 days. This time enables to clearly compare the effect of longitudinal dispersivity between the two examples. Results are benchmarked against the well-known FEM commercial code COMSOL Multiphysics. The same spatial discretization is used as in the case of lattice Boltzmann solution. We used direct UMFPACK time-dependent solver in COMSOL Multiphysics with relative tolerance of 0.01. In the first example a typical ratio of 10 between α_L and α_T is used with the dispersivity coefficients $\alpha_L = 0.1$ m and $\alpha_T = 0.01$ m with maximal cell Péclet number $Pe = 1$. These values represent large dissipation which results in a large spread over the domain. The results are shown in Fig. 6a. In order to demonstrate the potential of the presented approach, larger ratio between the longitudinal and transversal dispersivity of 1000 is shown in the second case. This case assumes larger longitudinal dispersivity $\alpha_L = 1$ m and lower transversal dispersivity $\alpha_T = 0.001$ m resulting in maximal cell Péclet number $Pe = 0.01$. As shown in Fig. 6b, the concentration field extends longitudinally more in the same time compared to the previous case due to larger longitudinal dispersivity. On the other hand, transversal dissipation perpendicular to the flow direction is lower as a consequence of lower transversal dispersivity.

Concentration profile on an outflow portion of a bottom boundary in Fig. 7 shows the magnitude of dispersion compared to the initial profile (black line) and shift of peak concentration towards the middle where the velocities are higher. Larger dissipation in transversal direction at the output is clearly observed in Fig. 7a compared to Fig. 7b. In both cases, the agreement with the reference solution is very good.

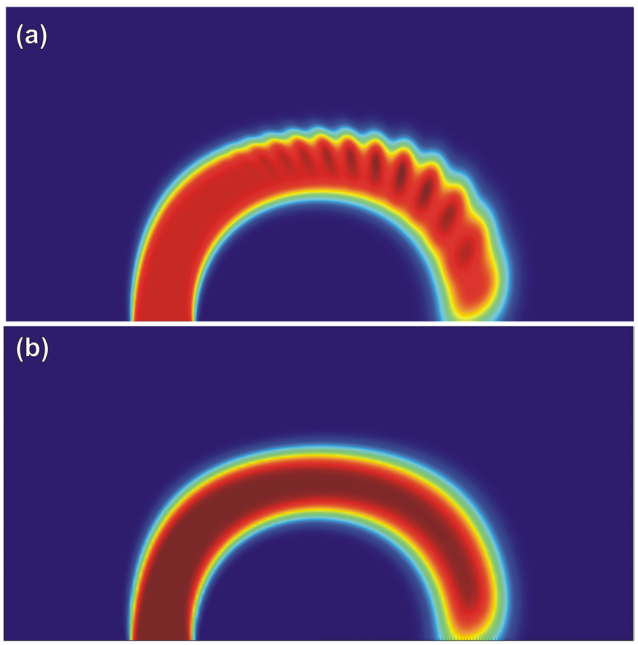

Fig. 8 Concentration field at time 1.7 days for **a** COMSOL Multiphysics solution and **b** LB-SRT solution. Color scale is denoted with blue and red colors for 0 and 1 concentrations, respectively

With lower dispersivity coefficients also, the dispersion decreases which leads to a higher Péclet number. This results in lower stability of the solution. In Fig. 8, we can clearly observe the unstable solution for $\alpha_L = 0.001$ m and $\alpha_T = 0.0001$ m obtained by COMSOL Multiphysics and stable solution obtained by the proposed formulation based on the above-mentioned simulation parameters at maximal cell Péclet number, $Pe = 8$.

4 Conclusions

In this paper, a new approach to implement anisotropic advection-dispersion equations into single-relaxation-time lattice Boltzmann method is presented. This approach is based on the diffusion velocity formulation, which is an alternative to the existing approaches using either multiple-relaxation rates collisions, or anisotropic equilibrium weights (or the combination of both). The described approach has the following properties: (1) Mass balance is preserved because the equilibrium function formulation remains the same as in classical SRT formulation. (2) The formulation is stable for large variations of dissipation parameters and anisotropy ratios as shown in the example where the anisotropy ratio is three orders of magnitude. (3) The model is straightforward to implement because the LB procedure and equilibrium function formulation remains the same. The only difference is the calculation of diffusion velocity $\mathbf{u}_d$, which is added to the usual advective vector. This model introduces two tuning parameters, the reference diffusion D_{ref} which is set on the basis of the desired time step and stability already discussed in [26] and τ. Analyses in this work show that the results are more accurate when adjusting D_{ref} while keeping the relaxation time $\tau = 1$ fixed. The reference diffusion is usually chosen to be equal to the molecular diffusion, but can be chosen differently in the cases with higher Pe to assure stability. The results also demonstrate that the accuracy of the solution does do not depend significantly on the level of anisotropy.

References

1. Anwar, S., Sukop, M.C.: Lattice Boltzmann models for flow and transport in saturated Karst. Ground Water **74**(3), 401–413 (2009)
2. Bear, J., Cheng, A.H.D.: Modeling Groundwater Flow and Contaminant Transport. Springer (2010)
3. Bhatnagar, P.L., Gross, E.P., Krook, M.: A model for collision processes in gases. I: small amplitude processes in charged and neutral one-component system. Phys. Rev. **94**, 511–525 (1954)
4. Chai, Z., Shi, B., Guo, Z.: A multiple-relaxation-time lattice Boltzmann model for general nonlinear anisotropic convection–diffusion equations. J. Sci. Comput. **69**, 355–390 (2016)
5. Dou, Z., Zhou, Z.: Lattice Boltzmann simulation of solute transport in a single rough fracture. Water Sci. Eng. **7**(3), 277–287 (2014)
6. Eker, E., Akin, S.: Lattice Boltzmann simulation of fluid flow in synthetic fractures. Transp. Porous Media **65**(3), 363–384 (2006)
7. Eshghinejadfard, A., Daróczy, L., Janiga, G., Thévenin, D.: Calculation of the permeability in porous media using the lattice Boltzmann method. Int. J. Heat Fluid Flow **62**(Part A), 93–103 (2016)
8. Flekkøy, E.G.: Lattice Bhatnagar-Gross-Krook models for miscible fluids. Phys. Rev. E **47**(6), 4247–4257 (1993)
9. Ginzburg, I.: Equilibrium-type and link-type lattice Boltzmann models for generic advection and anisotropic-dispersion equation. Adv. Water Resour. **28**(11), 1171–1195 (2005)
10. Ginzburg, I.: Truncation errors, exact and heuristic stability analysis of two-relaxation-times lattice Boltzmann schemes for anisotropic advection-diffusion equation. Commun. Comput. Phys. **11**(5), 1439–1502 (2012). https://doi.org/10.4208/cicp.211210.280611a
11. Ginzburg, I.: Multiple anisotropic collisions for advection-diffusion lattice Boltzmann schemes. Adv. Wat. Res. **51**, 381–404 (2013)
12. Ginzburg, I.: Prediction of the moments in advection-diffusion lattice Boltzmann method. II. Attenuation of the boundary layers via double-Λ bounce-back flux scheme. Phys. Rev. E **95**, 013,305 (2017). https://doi.org/10.1103/PhysRevE.95.013305
13. Ginzburg, I., Roux, L.: Truncation effect on Taylor-Aris dispersion in lattice Boltzmann schemes: accuracy towards stability. J. Comput. Phys. **299**, 974–1003 (2015)
14. Guo, Z., Zhao, T.S.: A lattice Boltzmann model for convection heat transfer in porous media. Numer. Heat Transfer Part B: Fund. **47**(2), 157–177 (2005). https://doi.org/10.1080/10407790590883405
15. Huang, R., Wu, H.: A modified multiple-relaxation-time lattice Boltzmann model for convection–diffusion equation. J. Comput. Phys. **274**, 50–63 (2014)
16. Krüger, T., Kusumaatmaja, H., Kuzmin, A., Shardt, O., Silva, G., Viggen, E.M.: Lattice Boltzmann for advection-diffusion Problems, pp. 297–329. Springer International Publishing, Cham (2017)
17. Lallemand, P., Luo, L.S.: Theory of the lattice Boltzmann method: dispersion, dissipation, isotropy, Galilean invariance, and stability. Phys. Rev. E **61**, 6546–6562 (2000)
18. Liu, H., Kang, Q., Leonardi, C.R., Schmieschek, S., Narváez, A., Jones, B.D., Williams, J.R., Valocchi, A.J., Harting, J.: Multiphase lattice Boltzmann simulations for porous media applications. Comput. Geosci. **20**(4), 777–805 (2016)
19. Maggiolo, D., Picano, F., Guarnieri, M.: Flow and dispersion in anisotropic porous media: a lattice-Boltzmann study. Phys. Fluids **28**(10), 102,001 (2016)
20. Montessori, A., Prestininzi, P., Rocca, M.L., Falcucci, G., Succi, S., Kaxiras, E.: Effects of Knudsen diffusivity on the effective reactivity of nanoporous catalyst media. J. Comput. Sci. **17**, 377–383 (2016). https://doi.org/10.1016/j.jocs.2016.04.006. http://www.sciencedirect.com/science/article/pii/S1877750316300448. Discrete Simulation of Fluid Dynamics 2015
21. Nourgaliev, R., Dinh, T., Theofanous, T., Joseph, D.: The lattice Boltzmann equation method: theoretical interpretation, numerics and implications. Int. J. Multiphase Flow **29**(1), 117–169 (2003)
22. Nützmann, G., Maciejewski, S., Joswig, K.: Estimation of water saturation dependence of dispersion in unsaturated porous media: experiments and modelling analysis. Adv. Water Resour. **25**(5), 565–576 (2002)
23. Oldenburg, C.M., Pruess, K.: Dispersive transport dynamics in a strongly coupled groundwater-brine flow system. Water Resour. Res. **31**(2), 289–302 (1995)
24. Patel, R.A., Phung, Q.T., Seetharam, S.C., Perko, J., Jacques, D., Maes, N., Schutter, G.D., Ye, G., Breugel, K.V.: Diffusivity of saturated ordinary portland cement-based materials: a critical

review of experimental and analytical modelling approaches. Cem. Concr. Res. **90**(Supplement C), 52–72 (2016)
25. Perko, J., Patel, R.A.: Diffusion velocity lattice Boltzmann formulation applied to transport in macroscopic porous media. Int. J. Modern Phys. C **25**(12), 1441,006 (2014)
26. Perko, J., Patel, R.A.: Single-relaxation-time lattice Boltzmann scheme for advection-diffusion problems with large diffusion-coefficient heterogeneities and high-advection transport. Phys. Rev. E **89**(053), 309 (2014)
27. Rasin, I., Succi, S., Miller, W.: A multi-relaxation lattice kinetic method for passive scalar diffusion. J. Comp. Phys. **206**(2), 453–462 (2005)
28. Silva, G., Talon, L., Ginzburg, I.: Low- and high-order accurate boundary conditions: from Stokes to Darcy porous flow modeled with standard and improved Brinkman lattice Boltzmann schemes. J. Comput. Phys. **335**(Supplement C), 50–83 (2017)
29. Smith, R.M., Hutton, A.G.: The numerical treatment of advection: A performance comparison of current methods. Numer. Heat Transfer **5**(4), 439–461 (1982)
30. Smolarkiewicz, P.K.: A simple positive definite advection scheme with small implicit diffusion. Month. Weather Rev. **111**(3), 479–486 (1983). https://doi.org/10.1175/1520-0493(1983)111<0479:ASPDAS>2.0.CO;2
31. Vikhansky, A., Ginzburg, I.: Taylor dispersion in heterogeneous porous media: extended method of moments, theory, and modelling with two-relaxation-times lattice Boltzmann scheme. Phys. Fluids **26**(2), 022,104 (2014). https://doi.org/10.1063/1.4864631
32. Walsh, S.D.C., Saar, M.O.: Interpolated lattice Boltzmann boundary conditions for surface reaction kinetics. Phys. Rev. E **82**(6), 066,703 (2010)
33. Yoshida, H., Nagaoka, M.: Multiple-relaxation-time lattice Boltzmann model for the convection and anisotropic diffusion equation. J. of Comp. Phys. **229**(20), 7774–7795 (2010)
34. Zhang, X., Bengough, A.G., Crawford, J.W., Young, I.M.: A lattice BGK model for advection and anisotropic dispersion equation. Adv. Water. Res. **25**, 1–8 (2002)